

Giant nonlinear response due to unconventional oscillation in Nodal-line semimetals

Debabrata Sinha^{1,2} and A. Taraphder¹

¹*Department of Physics, Indian Institute of Technology, Kharagpur-721302, India*

²*Institute of Mathematical Sciences, Taramani, Chennai 600113, India*

(Dated: September 9, 2021)

Quantum oscillations in magnetoconductance of a material at low temperatures and in presence of an intense magnetic field are described by the Shubnikov de Haas (SdH) effect. It is widely assumed to be the hallmark of the Fermi surface of a given metal. In contrast to the canonical situation, we identify an exotic oscillation in nonlinear responses of three-dimensional nodal line semimetals (NLSMs) which persist even at temperatures where the typical SdH-like oscillations vanish. This oscillation occurs due to the periodic gap-closing of a pair of Landau levels at zero Fermi energy with the variation of the magnetic field. The emergence of the oscillation is a remarkable fingerprint of ring dispersion and the corresponding frequency can be used to determine the radius of the ring. Using the Boltzmann equation, we calculate the second harmonic generation of nodal line semimetals under parallel DC electric and strong magnetic fields. The second harmonic conductivity diverges at the gap closing condition leading to the giant nonlinear response in NLSMs.

Introduction:- The interaction between solids and laser field induces innumerable nonlinear effects in a material¹⁻⁴. Among these, the second harmonic nonlinear effect occurs in a crystal without inversion symmetry. The nonlinear response became a basic tool to examine the various electronics properties such as dynamical Bloch oscillation⁵, quantum interference⁶ and band geometry^{7,8} of a given crystal. In recent years, the nonlinear effects of three-dimensional topological materials like Dirac and Weyl semimetals have drawn much attention⁹. The effects in those materials are found to be several times larger than the semiconductors or other conventional metals and yield potential applications for optical devices. Experimentally, a giant second-order nonlinear effect has been reported in inversion broken Weyl semimetals (WSMs) such as TaAs, TaP, and NbAs³. A large value of second-order nonlinear susceptibility $\chi^{(2)}$ predicted in Dirac semimetals and magnetic WSMs^{9,10}. Most of the intriguing nonlinear phenomena including quantized circular photogalvanic effect^{4,11}, shift current¹², photocurrent¹³ in three dimensional (3D) topological materials are stemmed from their low energy band structure.

Nodal line semimetals (NLSMs) are another class of 3D topological materials having linear dispersion around a one dimensional (1D) loop in k -space^{14,15}. These materials are distinct from other 3D topological materials like Weyl or Dirac in which the linear dispersion occurs around some discrete points in the Brillouin zone. Many nodal line materials have been found experimentally, like HgCr₂Se₄¹⁶, Cu₃(Pd/Zn)N^{17,18}, SrIrO₃¹⁹, Ca₃P₂²⁰ and ZrSiS²¹. The experimental characterization of their nodal loop structure can be probed by quantum oscillations (QOs) in presence of an external magnetic field²²⁻²⁵. The oscillation in resistivity, known as SdH oscillation, originated from the periodic crossing of quantized Landau levels (LLs) with chemical potential. The oscillation period is related to the shape of the Fermi surface. In addition to this, in NLSMs, a pair of LLs periodically intersects each other at zero Fermi energy

with a variation of the magnetic which violates the conventional QOs theory. This novel oscillation is a remarkable fingerprint of nodal line dispersion and it is absent in other topological materials like Dirac and Weyl semimetals. We ask the question: whether the exotic oscillation leads to any novel and technologically useful nonlinear properties in NLSM. Moreover, can there be similar SdH oscillation in nonlinear response which can probe the Fermi surface of NLSMs. This is because the hallmark of NLSM in nonlinear response is still missing.

In this Letter, we study the nonlinear responses in NLSM in presence of a strong magnetic field, using the semiclassical Boltzmann transport equation. A small DC electric field is introduced to break the inversion symmetry. We calculate the current induced second harmonic generation (SHG). The second harmonic conductivity (SHC) is found to exhibit oscillations with inverse magnetic field $1/B$ at temperature $T \rightarrow 0$. The oscillation is akin to the SdH oscillation in which extremal orbits are identified through the magnetic field dependence. At finite temperature, SHC diverges periodically with a variation of the inverse magnetic field $1/B$. The divergence occurs at the specific values of magnetic fields where a pair of LLs closes their gap at zero Fermi energy. The second harmonic nonlinear susceptibility $\chi(2\omega)$ has the largest value around those specific values of magnetic fields. We also predict this novel oscillation exists in higher harmonic generations of NLSMs.

Model Hamiltonian and LL Spectrum:- Let us consider a 3D NLSM Hamiltonian in low energy, is given by,^{23,26,27}

$$\mathcal{H} = ((p_x^2 + p_y^2)/2m^* - \Delta)\sigma_x + vp_z\sigma_z \quad (1)$$

where σ is the Pauli matrices acting on the orbital space, $m^* > 0$ is the effective mass, v is the Fermi velocity in the z -direction and $\Delta > 0$ is a constant in energy scale. The model Hamiltonian in Eq.(1) preserves both parity $\mathcal{P} = \sigma_x \otimes (\mathbf{k} \rightarrow -\mathbf{k})$ and time-reversal symmetry $\mathcal{T} = K \otimes (\mathbf{k} \rightarrow -\mathbf{k})$, where K is the complex conjugation.

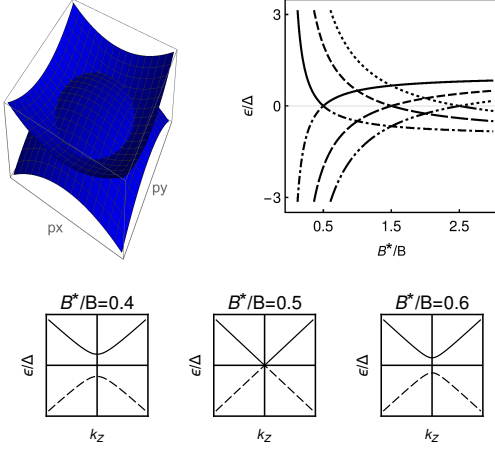


FIG. 1. Upper panel displays the zero magnetic field spectrum (in the left). Right hand side, we show the Landau level spectrum with inverse magnetic field. The crossing point of a pair of Landau Levels appear periodically with $1/B$. Lower panel displays $n = 0$ Landau level spectrum with increasing $1/B$ field. The Landau levels simplifies to a linear spectrum for $B^*/B = 0.5$.

The energy spectrum of the Hamiltonian is given by,

$$E_{\pm} = \pm \sqrt{(\Delta - (p_x^2 + p_y^2)/2m^*)^2 + v^2 p_z^2} \quad (2)$$

The upper and lower energy bands touches along a circle defined by $p_0^2 = p_x^2 + p_y^2 = 2m^*\Delta$, at $p_z = 0$ plane in BZ with a radius $\sqrt{2m^*\Delta}$. At low energy, the system Hamiltonian yields the Dirac cone at $\pm p_0$. The Fermi surface takes the shape of torus of genus one, for $\mu < \Delta$, where μ is the chemical potential. The Fermi surface has a drumlike structure for $\mu > \Delta$. Further increase of μ , the surface geometry changes to sphere of genus zero. We apply the magnetic field along z -direction i.e., $\mathbf{B} = (0, 0, B)$ and choose the vector potential is $\mathbf{A} = (-yB, 0, 0)$. Define ladder operators, $a \equiv -[(y - l_B^2 k_x)/l_B + l_B \partial_y]/\sqrt{2}$ and $a^\dagger \equiv -[(y - l_B^2 k_x)/l_B - l_B \partial_y]/\sqrt{2}$ with magnetic length $l_B = \sqrt{\hbar/eB}$. We can rewrite the Hamiltonian in Eq.(1) in terms of Ladder operators as follows,

$$\mathcal{H} = [\frac{\hbar e B}{m_*} (a^\dagger a + 1/2) - \Delta] \sigma_x + v p_z \sigma_z \quad (3)$$

The Landau eigenenergies of Eq.(3) are given by^{23,24},

$$\epsilon_n^\pm = \pm \sqrt{[\Delta - \frac{\hbar e B}{m_*} (n + 1/2)]^2 + v^2 p_z^2} \quad (4)$$

where $n = 0, 1, 2, \dots$ is the Landau index. The pairs of Landau Levels ϵ_n^+ and ϵ_n^- for a given n , crosses each others with the variation of magnetic field. The crossing occurs at a set of magnetic fields,

$$B_n = \frac{m^* \Delta}{e \hbar (n + 1/2)} \quad (5)$$

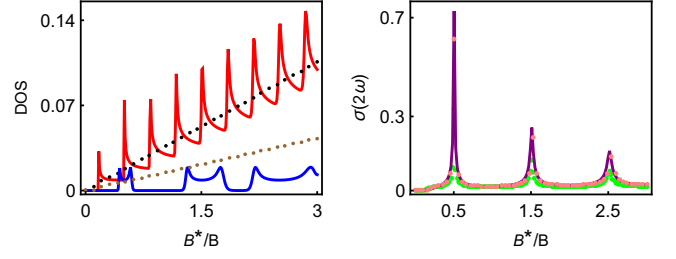


FIG. 2. Left Panel, displays the density of states (DOSs), in Eq.(16) of main text, with inverse magnetic field. The red and blue solid lines correspond to $\mu/\Delta = 2$ and 0.1 , respectively. The temperature is fixed at $k_B T/\Delta = .01$. The dotted lines are the corresponding classical natures at finite temperature, $k_B T/\Delta = 1$. Right panel, shows the second order conductivity $\sigma(2\omega)$ (in unit of $e^3 \tau/\hbar^2$) with inverse magnetic field for different μ . The temperature is fixed at $k_B T/\Delta = 1$, where the oscillations in DOS vanishes. The conductivity $\sigma(2\omega)$ diverges at the quantized value of $B^*/B = (n + 1/2)$, with $B^* = m^* \Delta/e\hbar$. Here, we take a finite value of mass $m/\Delta = 0.01$, to regularize the divergence in the peak. The purple solid line, green dotted line and black dashed line corresponds to $\mu/\Delta = .5, 1$ and 2 , respectively. See text for details.

In the rest of the paper we scale energy ϵ_n by Δ and magnetic field B by $B^* = m^* \Delta/e\hbar$.

Current induced SHG:- We calculate the response tensor of current induced second harmonic generation by using Boltzman transport equation. A weak DC electric field \mathbf{E}_{dc} is introduced which lead the system into a nonequilibrium steady state. In the relaxation time approximation, the steady state Boltzmann equation for the electron distribution f^n in the n -th Landau level is given by,

$$-\frac{e \mathbf{E}_{dc}}{\hbar} \cdot \nabla_{\mathbf{k}} f_{dc}^n = -\frac{f_{dc}^n - f_0^n}{\tau} \quad (6)$$

where $f_0^n = (e^{(\epsilon_n - \mu)/k_B T} + 1)^{-1}$, is the equilibrium distribution function. Here, k_B is the Boltzman constant, T is temperature and τ is the relaxation time. The solution with linear \mathbf{E}_{dc} of the above equation is given: $f_{dc}^n = f_0^n + \frac{e \tau \mathbf{E}_{dc}}{\hbar} \cdot \nabla_{\mathbf{k}} f_0^n$. Thus the DC electric field globally shift the Fermi surface by $\frac{e \tau \mathbf{E}_{dc}}{\hbar}$ in the \mathbf{k} -th direction. We now apply a strong laser beam of frequency ω and electric field amplitude \mathbf{E}_o . The total electric field is in the form $\mathbf{E}_{tot} = \mathbf{E}_{dc} + E_{op}(t) = \mathbf{E}_{dc} + \mathbf{E}_0 e^{-i\omega t} + c.c.$ The Boltzman equation in presence of both DC and optical field $E_{op}(t)$ is given by,

$$\frac{\partial f_{op}^n}{\partial t} - \frac{e(\mathbf{E}_{dc} + \mathbf{E}_{op}(t))}{\hbar} \cdot \nabla_{\mathbf{k}} f_{op}^n - \frac{e(\mathbf{E}_{dc} + \mathbf{E}_{op}(t))}{\hbar} \cdot \nabla_{\mathbf{k}} f_{dc}^n = -\frac{f_{dc}^n + f_{op}^n - f_0^n}{\tau} \quad (7)$$

Using Eq.(6) and considering weak DC field, the above

equation becomes^{10,28},

$$\frac{\partial f_{op}^n}{\partial t} - \frac{e\mathbf{E}_{op}(t)}{\hbar} \cdot \nabla_{\mathbf{k}} f_{op}^n - \frac{e\mathbf{E}_{op}(t)}{\hbar} \cdot \nabla_{\mathbf{k}} f_{dc}^n = -\frac{f_{op}^n}{\tau} \quad (8)$$

The distribution function f_{op}^n can be expanded in a power series in the electric field as follows,

$$f_{op}^n = f_{op}^{(n,\omega)} e^{-i\omega t} + f_{op}^{(n,2\omega)} e^{-2i\omega t} + \dots \\ + f_{op}^{(n,m\omega)} e^{-mi\omega t} + cc + ..$$

where $f_{op}^{(n,m\omega)} \propto \mathbf{E}_{op}^m$ is the m -th order corrections of the distribution function. In the following form,

$$f_{op}^{(n,\omega)} = \frac{e\tau\mathbf{E}_{op}}{\hbar(1-i\omega\tau)} \cdot \nabla_{\mathbf{k}} f_{dc}^n \\ f_{op}^{(n,2\omega)} = \frac{(e\tau)^2\mathbf{E}_{op}^2}{\hbar^2(1-i\omega\tau)(1-2i\omega\tau)} \nabla_{\mathbf{k}}^2 f_{dc}^n \\ \vdots \\ f_{op}^{(n,m\omega)} = \frac{(e\tau)^m\mathbf{E}_{op}^m}{\hbar^m(1-i\omega\tau)(1-2i\omega\tau)\dots(1-mi\omega\tau)} \nabla_{\mathbf{k}}^m f_{dc}^n \quad (9)$$

We consider the electric fields \mathbf{E}_{dc} and \mathbf{E}_{op} are along the z -direction i.e., $\mathbf{E}_{dc} \parallel \mathbf{B}$ and $\mathbf{E}_{op} \parallel \mathbf{B}$. So, we find only the z -component of charge density and zzz component of nonlinear conductivity tensor. The charge current density of the m -th order is given by,

$$j_z^{(n,m\omega)} = \frac{-e}{2\pi l_B^2} \sum_n \int v_{z,n} f^{(n,m\omega)} \frac{dk_z}{2\pi} \quad (10)$$

We obtain the linear response by using the distribution function in Eq.(9). Similarly, the second order response is derived by using Eq.(9) and the SHG current density is explicitly written as^{10,28},

$$j_z^{(n,2\omega)} = \frac{-e}{2\pi l_B^2} \frac{(e\tau\mathbf{E}_{op})^2}{\hbar^2(1-2i\omega\tau)(1-i\omega\tau)} \\ \sum_n \int v_{z,n} \nabla_{\mathbf{k}}^2 \left(f_0^n + \frac{e\tau E_{dc}}{\hbar} \frac{\partial f_0^n}{\partial k_z} \right) \frac{dk_z}{2\pi} \quad (11)$$

The first term in the integration $v_{l,n} \nabla_{\mathbf{k}}^2 f_0^n$ is zero since it is odd under $\mathbf{k} \rightarrow -\mathbf{k}$. Thus, the final form of SHG current density is given by,

$$j_z^{(n,2\omega)} = \frac{-e^4\tau^3\mathbf{E}_{op}^2 E_{dc}}{(2\pi l_B^2)\hbar^3(1-2i\omega\tau)(1-i\omega\tau)} \\ \sum_n \int v_{z,n} \frac{\partial^3 \epsilon_n}{\partial k_z^3} \frac{\partial f_0^n}{\partial \epsilon_n} \frac{dk_z}{2\pi} \quad (12)$$

Using the relation $j_l^{(n,2\omega)} = \sigma_{n,l}(2\omega)\mathbf{E}_{op}^2$, we obtained the second harmonic conductivity tensor $\sigma_{n,l}(2\omega)$:

$$\sigma(2\omega) = \frac{\sigma_{0z}}{(1-2i\omega\tau)(1-i\omega\tau)} \quad (13)$$

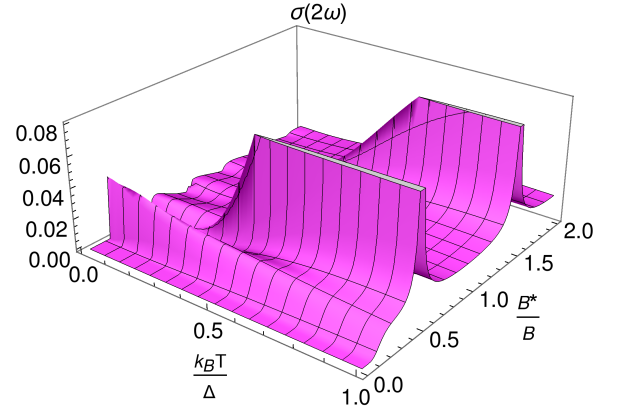


FIG. 3. The evolution of current induced SHC in NLSMs as a function of temperature and inverse magnetic field.

where,

$$\sigma_{0z} = \frac{1}{4\pi^2} \frac{B}{B^*} \frac{E_{dc}}{E_{dc}^*} \sum_n \int v_{z,n} \frac{\partial^3 \epsilon_n}{\partial k_z^3} \frac{\partial f_0^n}{\partial \epsilon_n} dk_z \quad (14)$$

Here, the conductivity σ_{0z} is scaled by $e^3\tau/\hbar^2$ and $E_{dc}^* = \hbar\Delta/e\tau^2 v^3 m^*$. The behaviour of quantum transport is controlled by the derivative of the Fermi function, which is given by,

$$\frac{\partial f_0^n}{\partial \epsilon} = -\frac{1}{2k_B T} \frac{1}{1 + \cosh\left[\frac{(\epsilon_n - \mu)}{k_B T}\right]} \quad (15)$$

which has a peak at $\epsilon_n = \mu$ with a width depends on temperature. We define the the density of states near the Fermi level^{29,30},

$$DOS = \frac{1}{2k_B T} \sum_n \frac{1}{1 + \cosh\left[\frac{(\epsilon_n - \mu)}{k_B T}\right]} \quad (16)$$

Results and Discussions:- The left panel of Fig.(2) displays the variation of DOS as a function of inverse magnetic field for two different chemical potentials. At sufficiently low temperature $k_B T \ll \hbar\omega_B = \hbar eB/m^*$, there are $1/B$ -periodic quantum oscillation in DOS. We find the periodicity in $1/B$ is $(1 + \mu/\Delta)^{-1}/B^*$ (shown by red solid line) for $\mu > \Delta$. On the other hand, for $\mu < \Delta$, the oscillation appears with two peaks. The peaks have different periodicities in $1/B$, which are $(1 + \mu/\Delta)^{-1}/B^*$ and $(1 - \mu/\Delta)^{-1}/B^*$, respectively (shown by blue solid line). The peak of the oscillation occurs in each time when a Landau level crosses the chemical potential. The double peaks are associated with two extremal Fermi surfaces of NLSMs for $\mu < \Delta$. As the temperature increased, the oscillation corresponding to Landau level gradually smoothed out as shown by black and brown dotted lines. When $k_B T \gg \hbar\omega_B$, the integration factor in Eq.(14) simplifies,

$$\sum_n \int v_{z,n} \frac{\partial^3 \epsilon_n}{\partial k_z^3} \frac{\partial f_0^n}{\partial \epsilon_n} dk_z \simeq \frac{\pi}{64k_B T} \sum_n \frac{\text{Sech}^2\left(\frac{|\mathcal{B}_n| - \mu}{2k_B T}\right)}{|\mathcal{B}_n|} \quad (17)$$

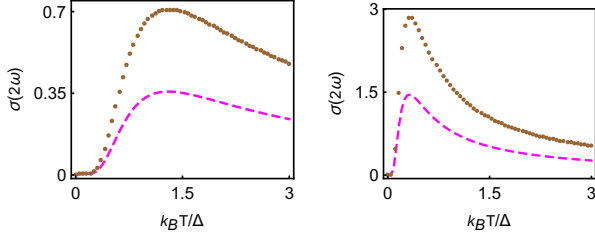


FIG. 4. **Temperature Dependence:** $\sigma(2\omega)$ is plotted against temperature $k_B T/\Delta$ for $\mu > \Delta$ (left panel) ($\mu/\Delta = 2$) and $\mu < \Delta$ (right panel) ($\mu/\Delta = 0.5$). In both panels the brown dotted line and magenta solid line correspond to $m/\Delta = .005$ and $.01$, respectively. We fixed the value $B^*/B = 0.5$ in both panels.

where $\mathcal{B}_n = (1 - B(n + 1/2)/B^*)$. The right hand side function in Eq.(17) has singularities at $\mathcal{B}_n \rightarrow 0$ i.e., $B^*/B = (n + 1/2)$. As a result, the conductivity tensor $\sigma(2\omega)$ diverges periodically with an inverse magnetic field with periodicity $1/B = e\hbar/m^*\Delta$. This is one of the main results of our work. We have shown this in the right panel of Fig.(2). We consider a \mathcal{PT} breaking mass term ($m\sigma_y$) in the Hamiltonian in Eq.(1) to regularize the divergence^{26,27}. The right hand side of Eq.(17) now modifies to:

$$\frac{\pi}{64k_B T} \sum_n \frac{\text{Sech}^2\left(\frac{\sqrt{m^2 + \mathcal{B}_n^2} - \mu}{2k_B T}\right)}{\sqrt{m^2 + \mathcal{B}_n^2}} \quad (18)$$

. This quantity diverges at $m \rightarrow 0$ and $\mathcal{B}_n \rightarrow 0$, which appears periodically with $1/B$. The frequency of this oscillation is μ independent.

From Eq.(5), the LLs of given index n simplifies to a linear spectrum at the specific values of magnetic field: $B^*/B_n = (n + 1/2)$. The pair of n -th LLs intersect each other at zero Fermi energy and the gap vanishes. Consequently, the conductivity $\sigma_n(2\omega)$ and higher-order conductivities will vanish since they involve higher-order derivatives (see Eq.(12)). The linear spectrum occurs for each Landau index n which gives rise to a μ -independent oscillation. This is in contrast to Weyl or Dirac semimetals where the linear dispersion only appears for $n = 0$ ³². However, this oscillation gets suppressed by the SdH oscillation, shown in Fig.(3). This is because at Low temperature, Eq.(15) becoming a delta function, signifies that only near the Fermi surface electron's contributes to the SHG. As a result, the function in Eq.(17) does not diverge and only SdH oscillation persists. With increasing the temperature, electrons deep in the Fermi sphere are also taken into the process of SHG. That makes the function in Eq.(17) divergent at $\mathcal{B}_n \rightarrow 0$ and at finite temperature.

We show the temperature dependence of $\sigma(2\omega)$ in Fig.(4), with different mass values m and for a fixed value of $B^*/B = 0.5$. The amplitudes of $\sigma(2\omega)$ increases with temperature upto a maximum value and then decreases. The maximum amplitude of $\sigma(2\omega)$ diverges at $m \rightarrow 0$.

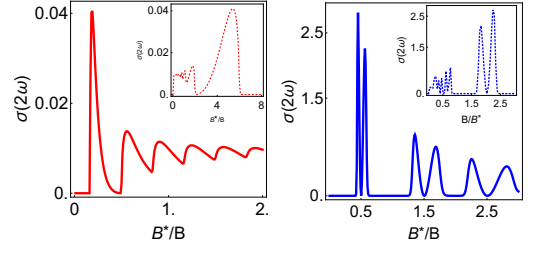


FIG. 5. The total second harmonic conductivity $\sigma(2\omega)$ as a function of inverse magnetic field at $k_B T/\Delta = 0.01$. We fix $\mu/\Delta = 2$ and $\mu/\Delta = .15$ in the left and right panel, respectively. Inset shows the variation of $\sigma(2\omega)$ with magnetic field.

The temperature T_d at which $\sigma(2\omega)$ has largest value can be determined from the condition: $\frac{d\sigma_{0z}}{dT}|_{T=T_d} = 0$ with $m \rightarrow 0$ and $\mathcal{B}_n \rightarrow 0$. We find, $k_B T_d/\Delta \simeq .64\mu/\Delta$.

We now discuss the origin of quantum oscillations in SHC at Low temperature which are shown in Fig.(5). At low temperature, $\frac{\partial f_0^n}{\partial \epsilon} = -\delta(\epsilon_n - \mu)$, and Eq.(14) simplifies to,

$$\sigma_{0l} = \frac{3}{4\pi^2} \frac{B}{B^*} \frac{E_{dc}}{E_{dc}^*} \left(\frac{k_F^3}{|\mu|^5} - \frac{k_F}{|\mu|^3} \right) \quad (19)$$

where $k_F = \sqrt{(\mu/\Delta)^2 - (1 - B(n + 1/2)/B^*)^2}$ is the Fermi wave vector. It becomes zero for two magnetic fields: $B_n^\pm = (1 \pm \mu/\Delta)B^*/(n + 1/2)$, in n -th LL. The magnetic fields B_n^\pm are real and finite for $\mu/\Delta < 1$. For $\mu/\Delta = 1$, the magnetic field B_n^- is zero but B_n^+ has a real finite value. With $\mu/\Delta > 1$, there is no real solution of B_n^- in the $k_F = 0$ equation. This unique nature of k_F is originated from the torus-like Fermi surface with two extremal surfaces S_1 and S_2 (shown in Fig.(6)). The energy dispersion for these extremal orbits (at $k_z = 0$) reduces to $\epsilon_\pm = |\hbar^2(k_x^2 + k_y^2)/2m_* - \Delta|$. With increasing values of μ , the surface S_2 (S_1) diminishes (increases) and finally vanishes at $\mu = \Delta$. Consequently, there is only a single extremal surface S_1 remains for $\mu > \Delta$. The area of cyclotron orbit A in k -space of n -th LL satisfies,

$$\frac{\mathcal{A}\hbar}{e} \frac{1}{B} = 2\pi(n + \gamma) \quad (20)$$

where $0 \leq \gamma < 1$ is related to the Berry phase of that orbit. The frequency of quantum oscillation with the variation of $1/B$ is given by $F = \mathcal{A}_F \hbar / (2\pi e)$, where \mathcal{A}_F is the cross section of extremal Fermi surface. We find the oscillation frequencies are $F_{S_1} = B^*(1 + \mu/\Delta)$ for outer circle and $F_{S_2} = B^*(1 - \mu/\Delta)$ for inner circle, respectively. The finite temperature oscillation of NLSMs corresponds to the area $\mathcal{A} = 0$ in k -space. However, the $1/B$ periodicity is governed by the area $\mathcal{A}_0 = \pi p_0^2$.

In Fig.(5) we show the variation of second harmonic conductivity $\sigma(2\omega)$ as a function inverse magnetic field ($1/B$) $\mu > \Delta$ and $\mu < \Delta$. The variation of $\sigma(2\omega)$ with magnetic field is shown in the inset. The conductivity $\sigma(2\omega)$ with magnetic field exhibits oscillation where

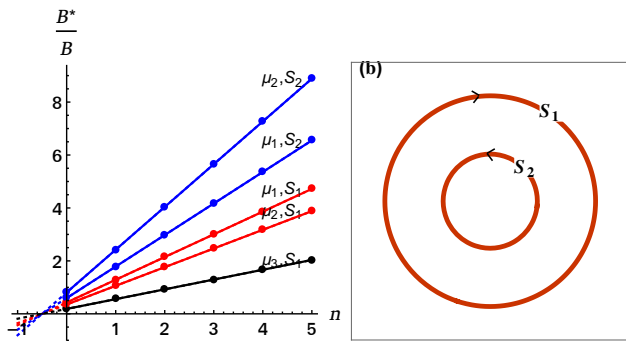


FIG. 6. Landau index n is plotted against peak position (B^*/B) for three different chemical potentials values $\mu_3 > \mu_2 > \mu_1$ and two corresponding cross sectional area $S_{1,2}$. The value of chemical potentials are $\mu_3/\Delta = 2$ (black line), $\mu_2/\Delta = 0.5$ (blue and red lines) and $\mu_1/\Delta = 0.2$ (blue and red lines). The temperature fixed at $k_B T/\Delta = 0.01$. Right panel shows the two surfaces S_1 and S_2 .

the amplitude increases with B . The oscillation occurs each time when a Landau level crosses the chemical potential, contributing a single peak in the conductivity. Each peak corresponds to the intraband transition in the Landau subbands. The higher Landau level contributes most to the $\sigma(2\omega)$ with decreasing magnetic field. As the magnetic field strength increases the lower Landau level starts to contribute. In the strong magnetic field regime when the Fermi level crosses lowest Landau level $n = 0$, we have a cutoff value of magnetic field B_c . The Fermi wave vector k_F becomes imaginary for any Landau subband n when $B > B_c = 2(1 + \mu/\Delta)B^*$. Consequently, the conductivity $\sigma(2\omega)$ vanishes if $B > B_c$. The periodicity of $\sigma(2\omega)$ with $1/B$ is given by, $(1/B)_{n+1} - (1/B)_n = 1/[B^*(1 + \mu/\Delta)]$. We find the oscillation period is $\approx .33/B^*$ for a given value of $\mu/\Delta = 2$. On the other hand, for $\mu/\Delta < 1$, the oscillation in $\sigma(2\omega)$ appears with two peaks with periodicity $\Delta(1/B) = 1/B^*(1 - \mu/\Delta)$ and $\Delta(1/B) = 1/B^*(1 + \mu/\Delta)$, respectively. We find oscillation frequencies $\Delta(1/B) = .88/B^*$ and $\Delta(1/B) = 1.15/B^*$ for a given value of $\mu/\Delta = 0.15$.

Fig.(6) displays the Landau index plot, n with peak

position B^*/B of SHC for three different values of μ ($\mu_3 > \mu_2 > \mu_1$). From Eq.(20), the Landau index n is linearly proportional to $1/B$ for a given cross-sectional area A . The slope of the $1/B$ vs n -lines is proportional to the inverse of cross sectional area and the intercept of this line on the n -axis determines the value $-\gamma$. The value of $\gamma = 0$ and $\gamma = 1/2$ corresponds to Berry phase 0 (trivial oscillation) and π (topological oscillation)²², respectively. Fig.(6) shows three fundamental frequencies. Two blue lines belong to the same frequency group, equal to $1/B^*(1 - \mu/\Delta)$. Two red lines and black lines in Fig.(6) belong to the other frequency group, equal to $1/B^*(1 + \mu/\Delta)$. All the lines in Fig.(6) show common intersections ($-1/2$) on the n -axis, indicating no Berry phase³¹⁻³⁵.

We estimate the strength of current induced SHG by evaluating the nonlinear susceptibility $\chi(2\omega) = \sigma(2\omega)/2i\omega\epsilon_0$, where ϵ_0 is the vacuum permittivity. The susceptibility takes the largest value at the gap closing condition i.e., $B^*/B = (n + 1/2)$. Considering, $m^* = 0.1m_e$ (m_e is the electron's rest mass), $\Delta = 0.01$ eV and $\tau = 10^{-13}$ s, we obtain $B^* \simeq 9$ T and $E_{dc}^* \simeq 10^3$ V/m, respectively. We take the frequency of the probe light $\omega = 0.5$ THz and the optical field $E_{op} = 10^4$ V/m. For a magnetic field value $B \simeq 6$ T and $\mu = 20$ meV, we obtain $j(2\omega) = \sigma(2\omega)E_{op}^2 \simeq 10^6$ A/m² at low temperature $T = 1$ K and $j(2\omega) \simeq 10^8$ A/m² at high temperature $T = 150$ K. We find $\chi(2\omega) \simeq 10^4$ pm/V and $\chi(2\omega) \simeq 10^6$ pm/V at temperature $T = 1$ K and $T = 150$ K, respectively. These values of susceptibility are large compared to the value found in WSMs^{3,10}.

Conclusions:- We uncover an unusual mechanism for the realization of giant nonlinear response in NLSMs at finite temperature. This giant response occurs near specific values of magnetic fields for which Landau levels simplify to a linear spectrum. We find SdH oscillation in SHG which may probe the Fermi surface of NLSMs. We hope our findings will prompt further investigation of the nonlinear effect in NLSMs for technological applications.

Acknowledgement:- D.S. acknowledge T. K. Bose for initial collaboration.

Note:- During preparation of the manuscript we noticed Ref.³⁷ where similar oscillation are studied but not for nonlinear responses.

¹ N. Bloembergen, Nonlinear Optics, 4th ed. (World Scientific, Singapore, 1996)

² Y. Bai, F. Fei, S. Wang, N. Li, X. Li, F. Song, R. Li, Z. Xu and P. Liu, High-harmonic generation from topological surface states, Nat. Phys. 17, 311 (2021)

³ L. Wu, S. Patankar, T. Morimoto, N. L. Nair, E. The-walt, A. Little, J. G. Analytics, J. E. Moore, and J. Orenstein, Giant anisotropic nonlinear optical response transition metal monopnictide Weyl semimetals, Nat. Phys. 13, 350 (2017)

⁴ F. de Juan, A. G. Grushin, T. Morimoto, and J. E. Moore,

Quantized circular photogalvanic effect in Weyl semimetals, Nature Communications 8, 15995 (2017)

⁵ O. Schubert, M. Hohenleutner, F. Langer, B. Urbanek, C. Lange, U. Huttner, T. Meier, M. Kira, S. W. Koch and R. Huber, Sub-cycle control of terahertz high-harmonic generation by dynamical Bloch oscillation, Nat. Photon. 8, 119-123 (2014)

⁶ M. Hohenleutner, F. Langer, M. Knorr, U. Huttner, S. W. Koch, M. Kira and R. Huber, Real-time observation of interfering crystal electrons in high-harmonic generation, Nature 523, 572-575 (2015)

- ⁷ I. Sodemann and L. Fu, Quantum Nonlinear Hall Effect Induced by Berry Curvature Dipole in Time-Reversal Invariant Materials, *Phys. Rev. Lett* 115, 216806 (2015)
- ⁸ J. E. Moore and J. Orenstein, Confinement-Induced Berry Phase and Helicity-Dependent Photocurrents, *Phys. Rev. Lett.* 105, 026805 (2010)
- ⁹ K. Takasan, T. Morimoto, J. Orenstein, and J. E. Moore, Current-induced second harmonic generation in inversion-symmetric Dirac and Weyl semimetals, arXiv 2007.08887
- ¹⁰ Y. Gao and F. Zhang, Current-induced second harmonic generation of Dirac or Weyl semimetals in a strong magnetic field, *Phys. Rev. B* 103, L041301 (2021)
- ¹¹ F. Flicker, F. d. Juan, B. Bradlyn, T. Morimoto, M. G. Vergniory, and A. G. Grushin, Chiral optical response of multifold fermions, *Phys. Rev. B* 98, 155145 (2018)
- ¹² G. B. Osterhoudt, L. K. Diebel, M. J. Gray, X. Yang, J. Stanco, X. Huang, B. Shen, N. Ni, P. J. W. Moll, Y. Ran and K. S. Burch, Colossal mid-infrared bulk photovoltaic effect in a type-I Weyl semimetal, *Nat. Materials* 18, 471-475 (2019)
- ¹³ C.-K. Chan, N. H. Lindner, G. Refael, and P. A. Lee, Photocurrents in Weyl semimetals, *Phys. Rev. B* 95, 041104(R) (2017)
- ¹⁴ C. Fang, Y. Chen, H.-Y. Kee, and L. Fu, Topological nodal line semimetals with and without spin-orbital coupling, *Phys. Rev. B* 92, 081201(R) (2015)
- ¹⁵ A. A. Burkov, M. D. Hook, and L. Balents, Topological nodal semimetals, *Phys. Rev. B* 84, 235126 (2011)
- ¹⁶ G. Xu, H. M. Weng, Z. J. Wang, X. Dai, and Z. Fang, Chern Semimetal and the Quantized Anomalous Hall Effect in HgCr_2Se_4 , *Phys. Rev. Lett.* 107, 186806 (2011).
- ¹⁷ R. Yu, H. Weng, Z. Fang, X. Dai, and X. Hu, Topological Node-Line Semimetal and Dirac Semimetal State in Antiperovskite Cu_3PdN , *Phys. Rev. Lett.* 115, 036807 (2015)
- ¹⁸ Y. Kim, B. J. Wieder, C. L. Kane, and A. M. Rappe, Dirac Line Nodes in Inversion-Symmetric Crystals, *Phys. Rev. Lett.* 115, 036806 (2015).
- ¹⁹ Y. Chen, Y.-M. Lu, and H.-Y. Kee, Topological crystalline metal in orthorhombic perovskite iridates, *Nat. Commun.* 6, 6593 (2015).
- ²⁰ Y.-H. Chan, C.-K. Chiu, M. Y. Chou, and A. P. Schnyder, Ca_3P_2 and other topological semimetals with line nodes and drumhead surface states, *Phys. Rev. B* 93, 205132 (2016).
- ²¹ L. M. Schoop, M. N. Ali, C. Straßer, A. Topp, A. Varykhalov, D. Marchenko, V. Duppel, S. S. P. Parkin, B. V. Lotsch, and C. R. Ast, Dirac cone protected by nonsymmorphic symmetry and three-dimensional Dirac line node in ZrSiS , *Nat. Commun.* 7, 11696 (2016).
- ²² L. Oroszlany, B. Dora, J. Cserti, and A. Cortijo, Topological and trivial magnetic oscillations in nodal loop semimetals, *Phys. Rev. B* 97, 205107 (2018)
- ²³ H. Yang, R. Moessner and L.-K. Lim, Quantum oscillation in nodal line systems, *Phys. Rev. B* 97, 165118 (2018)
- ²⁴ C. Li, C. M. Wang, B. Wan, X. Wan, H.-Z. Lu and X. C. Xie, Rules for Phase Shifts of Quantum Oscillations in Topological Nodal-line Semimetals, *Phys. Rev. Lett* 120, 146602 (2018)
- ²⁵ S. Kar, Quantum oscillation and Landau-Zener transition in untilted nodal line semimetals under a time-periodic magnetic field, *J. Phys.: Condens. Matter* 33, 225601 (2021)
- ²⁶ A. M.-Ruiz and A. Cortijo, Parity anomaly in the nonlinear response of nodal-line semimetals, *Phys. Rev. B* 98, 155125 (2018)
- ²⁷ W. B. Rui, Y. X. Zhao, and A. P. Schnyder, Topological transport in Dirac nodal-line semimetals, *Phys. Rev. B* 97, 161113(R) (2018)
- ²⁸ J. L. Cheng, N. Vermeulen, and J. E. Sipe, DC current induced second order optical nonlinearity in graphene, *Opt. Express* 22, 15868 (2014)
- ²⁹ J. Knolle and N. R. Cooper, Anomalous de Haas-van Alphen Effect in InAs/GaSb Quantum Wells, *Phys. Rev. Lett* 118, 176801 (2017)
- ³⁰ L. Zhang, X.-Y. Song, F. Wang, Quantum Oscillation in Narrow-Gap Topological Insulators, *Phys. Rev. Lett* 116, 046404 (2016)
- ³¹ J.-W. Rhim and Y. B. Kim, Landau level quantization and almost flat modes in three-dimensional semimetals with nodal ring spectra, *Phys. Rev. B* 92, 045126 (2015)
- ³² M.-X. Deng, G. Y. Qi, R. Ma, R. Shen, R.-Q. Wang, L. Sheng, and D. Y. Xing, Quantum Oscillations of the Positive Longitudinal Magnetoconductivity: A Fingerprint for Identifying Weyl Semimetals, *Phys. Rev. Lett* 122, 036601 (2019)
- ³³ C. M. Wang, H.-Z. Lu, and S.-Q. Shen, Anomalous Phase Shift of Quantum Oscillations in 3D Topological Semimetals, *Phys. Rev. Lett* 117, 077201 (2016)
- ³⁴ Y. H. Kwan, P. Reiss, Y. Han, M. Bristow, D. Prabhakaran, D. Graf, A. McCollam, S. A. Parameswaran, and A. I. Coldea, Quantum oscillations probe the Fermi surface topology of the nodal-line semimetal CaAgAs , *Phys. Rev. Research* 2, 012055(R) (2020)
- ³⁵ J. Hu, Z. Tang, J. Liu, Y. Zhu, J. Wei, and Z. Mao, Nearly massless Dirac fermions and strong Zeeman splitting in the nodal-line semimetal ZrSiS probed by de Haas-van Alphen quantum oscillations, *Phys. Rev. B* 96, 045127 (2017)
- ³⁶ C. H. Lee, H. H. Yap, T. Tai, G. Xu, X. Zhang, and J. Gong, Enhanced higher harmonic generation from nodal topology, *Phys. Rev. B* 102, 035138 (2020)
- ³⁷ T. Devakul, Yves H. Kwan, S. L. Sondhi, S. A. Parameswaran, "Quantum oscillations in the zeroth Landau Level and the serpentine Landau fan", arXiv 2101.05294